

Kinematics and Host-Galaxy Properties Suggest a Nuclear Origin for Calcium-Rich Supernova Progenitors

Ryan J. Foley^{1,2*}

¹*Astronomy Department, University of Illinois at Urbana-Champaign, 1002 W. Green Street, Urbana, IL 61801, USA*

²*Department of Physics, University of Illinois at Urbana-Champaign, 1110 W. Green Street, Urbana, IL 61801, USA*

Accepted . Received ; in original form

ABSTRACT

Calcium-rich supernovae (Ca-rich SNe) are peculiar low-luminosity SNe Ib with relatively strong Ca spectral lines at ~ 2 months after peak brightness. This class also has an extended projected offset distribution, with several members of the class offset from their host galaxies by 30 – 150 kpc. There is no indication of any stellar population at the SN positions. Using a sample of 13 Ca-rich SNe, we present kinematic evidence that the progenitors of Ca-rich SNe originate near the centers of their host galaxies and are kicked to the locations of the SN explosions. Specifically, SNe with small projected offsets have large line-of-sight velocity shifts as determined by nebular lines, while those with large projected offsets have no significant velocity shifts. Therefore, the velocity shifts must not be primarily the result of the SN explosion. There is an excess of SNe with blueshifted velocity shifts within two isophotal radii (5/6 SNe), indicating that the SNe are moving away from their host galaxies and redshifted SNe on the far sides of their galaxies are selectively missed in SN surveys. Additionally, nearly every Ca-rich SN is hosted by a galaxy with indications of a recent merger and/or is in a dense environment. At least 6–7 host galaxies also host an AGN, a relatively high fraction, again linking the nuclear region of these galaxies to explosions occurring tens of kpc away. We propose a progenitor model which fits all current data: The progenitor system for a Ca-rich SN is a double white dwarf (WD) system where at least one WD has a significant He abundance. This system, through an interaction with a super-massive black hole (SMBH) is ejected from its host galaxy and the binary is hardened, significantly reducing the merger time. After 10 – 100 Myr (on average), the system explodes with a large physical offset. The rate for such events is significantly enhanced for galaxies which have undergone recent mergers, potentially making Ca-rich SNe new probes of both the galaxy merger rate and (binary) SMBH population.

Key words: supernovae—general, supernovae—individual (SN 2000ds, SN 2001co, SN 2003H, SN 2003dg, SN 2003dr, SN 2005E, SN 2005cz, SN 2007ke, SN 2010et, SN 2012hn, PTF09dav, PTF11bij, PTF11kmb), galaxies—individual (2MASS J22465295+2138221, CGCG 170-011, IC 3956, NGC 1032, NGC 1129, NGC 2207, NGC 2272, NGC 2768, NGC 4589, NGC 5559, NGC 5714, NGC 7265, UGC 6934)

1 INTRODUCTION

For the past century, systematic supernova (SN) searches have discovered thousands of SNe. Nearly all of these SNe fall into 3 classes: Type Ia, Type II, and Type Ib/c. However, over the last decade with the implementation of large SN searches, we have begun to discover many astrophysical transients that do not fall into the well-delineated

classes mentioned above. It turns out that there were about a dozen new classes of “exotic” or “peculiar” transients lurking in the shadows. These classes include luminous SNe IIn (e.g., Smith et al. 2007), Type I superluminous SNe (Quimby et al. 2011), kilonovae (Berger et al. 2013; Tanvir et al. 2013), SNe Iax (Foley et al. 2013), and SN 2006bt-like SNe (Foley et al. 2010).

One class, the SN 2005E-like SNe (Perets et al. 2010, hereafter, P10), also known as “Calcium-rich SNe” (or simply “Ca-rich SNe”; Filippenko et al. 2003; Kasliwal et al.

* E-mail: rfoley@illinois.edu

2012, hereafter, K12), are particularly interesting. These SNe are technically of Type Ib, having distinct He lines in their spectra near maximum brightness. However, they are less luminous and faster fading than normal SNe Ib (P10; K12) and are often found in early-type galaxies (P10; Lyman et al. 2013). Additionally, several members of the class, including SN 2005E have large projected offsets (>10 kpc and up to at least 150 kpc) from their host galaxies (P10; K12; Yuan et al. 2013; Lyman et al. 2014; this work).

Relative to other SNe Ib, Ca-rich SNe also have a distinct spectroscopic evolution. After about 2 months, the SNe show strong forbidden lines, indicating that the ejecta are at that point mostly optically thin. This is a much faster transition than for most SNe Ib. This “nebular” spectrum is also distinct, showing extremely strong [Ca II] $\lambda\lambda 7291, 7324$ emission relative to that of [O I] $\lambda\lambda 6300, 6363$, giving the name to the class (Filippenko et al. 2003). Modeling of the ejecta also indicates that the mass-fraction of Ca in the ejecta is also extremely high ($\sim 1/3$; P10).

P10 examined the rate of Ca-rich SNe in the Lick Observatory Supernova Search (LOSS; Filippenko et al. 2001), finding that they occur at $7 \pm 5\%$ the rate of SNe Ia. K12 found a rate $>2.3\%$ that of SNe Ia for the Palomar Transient Factory (PTF) sample. Therefore, Ca-rich SNe are somewhat common events and cannot come from extremely rare progenitor scenarios.

Since most Ca-rich SNe have early-type hosts (P10; Lyman et al. 2013), a massive star origin is unlikely. Moreover, there is no indication of star formation at the position of the SNe in deep pre- or post-explosion imaging (P10; Perets et al. 2011; K12; Lyman et al. 2014).

Because of the large offset distribution, it has been suggested that Ca-rich SNe occur in dwarf galaxies (K12; Yuan et al. 2013) or globular clusters (Yuan et al. 2013); however, the deep limits on any stellar light at the position of the SNe rule out such possibilities (Lyman et al. 2014). These observations require that the progenitors of Ca-rich SNe be born elsewhere and travel a significant distance to where they explode (Lyman et al. 2014). With this determination, Lyman et al. (2014) suggested that Ca-rich SN progenitors were neutron star (NS) – white dwarf (WD) binary systems which are kicked by the SN that created the NS and then undergo a merger after traveling far from their birth site.

In this manuscript, we present a kinematic and host-galaxy study of Ca-rich SNe. By examining the velocity shift distribution, the projected offset distribution, and the angle offset distribution, as well as the host-galaxy properties of the sample, we constrain the progenitor systems and origin of Ca-rich SNe. In Sections 2 and 3, we define our SN sample and discuss their host-galaxy properties. In Sections 4 and 5, we measure the projected offset and velocity shift distributions for our sample. In Section 6, we analyze these data. We present a basic progenitor model in Section 7. We discuss our results and summarize our conclusions in Section 8.

2 SUPERNOVA SAMPLE

Our sample consists of all known (and published) Ca-rich SNe. We begin with the Lyman et al. (2014) sample of Ca-rich SNe. This sample includes 12 SNe originally reported

in other works (P10; Kawabata et al. 2010; Sullivan et al. 2011; K12; Valenti et al. 2014). We include PTF09dav in this analysis, although at maximum light, it had much lower ejecta velocities than other members (Sullivan et al. 2011) and uniquely displays hydrogen emission at late-times (K12).

To this sample, we add PTF11kmb. PTF11kmb was discovered on 24.24 August 2011 (all times are UT) by PTF (Gal-Yam et al. 2011). A Keck/LRIS spectrum obtained 28 August 2011 was used to classify PTF11kmb as a SN Ib (Gal-Yam et al. 2011). We use this spectrum as well as a Keck/LRIS spectrum from 26.37 November 2011 to classify PTF11kmb as a Ca-rich SN (Appendix A).

Basic host-galaxy information was obtained through the NASA/IPAC Extragalactic Database (NED) and is presented in Table A1. Four SNe have somewhat ambiguous hosts, and we discuss each below.

SN 2003H occurred between two merging galaxies, NGC 2207 and IC 2163. Their recession velocities differ by 24 ± 25 km s $^{-1}$, and this difference does not affect our results. SN 2003H is offset by 8.73 and 5.75 kpc from NGC 2207 and IC 2163, respectively, and the difference in offset does not affect any results.

SN 2007ke occurred in a cluster environment (AWM 7) near the brightest member, NGC 1129. It is also near a group member, MCG+07-07-003. The difference in their recession velocities is 227 ± 23 km s $^{-1}$, with NGC 1129 having the larger redshift. This difference does not affect any results, but is noteworthy. The SN was offset by 16.71 and 8.20 kpc from NGC 1129 and MCG+07-07-003, respectively. Again, this difference does not affect any results. Given the relative sizes of these galaxies and large offset from MCG+07-07-003, NGC 1129 is a reasonable choice for the host galaxy. Nonetheless, given the cluster environment, it is possible that SN 2007ke originated from a faint cluster member or was formed in the intracluster medium.

SN 2010et occurred 37.6 – 69.2 kpc from three galaxies at redshifts consistent with the SN redshift. The closest galaxy, CGCG 170-011 is also relatively large. Using the NED reported major and minor 2MASS K_s isophotal axes (with a reference value of $K_s = 20.0$ mag arcsec $^{-2}$) and position angle, SN 2010et was offset 5.5 isophotal radii from CGCG 170-011. SN 2010et is 69.2 kpc and 16.5 isophotal radii from the other nearby, large galaxy, CGCG 170-010. A third galaxy, SDSS J171650.20+313234.4, is 46.9 kpc and is too small and faint for a 2MASS isophotal measurement. Based on offset, the most likely host is CGCG 170-011, and we assume this for the rest of the analysis. K12 determined that no source exists at the position of SN 2010et with $M_R < -12.1$ mag, but this does not completely rule out a possible dwarf galaxy as the host of SN 2010et.

Finally, PTF11kmb is far from any galaxy. PTF11kmb has a redshift of roughly $z = 0.017$ as determined by SN features (Gal-Yam et al. 2011, and confirmed in our analysis). The closest galaxy listed in NED is 4.2 arcmin away and has no redshift information. However, if it is at the distance of PTF11kmb, it would be offset by ~ 80 kpc. The three closest galaxies with redshifts are 2MASX J22224094+3613514 (offset by 4.5 arcmin, 83.0 kpc, and 36.6 isophotal radii; $cz = 4500 \pm 25$ km s $^{-1}$), UGC 12007 (offset by 6.5 arcmin, 127.3 kpc, and 15.0 isophotal radii; $cz = 4829 \pm 33$ km s $^{-1}$),

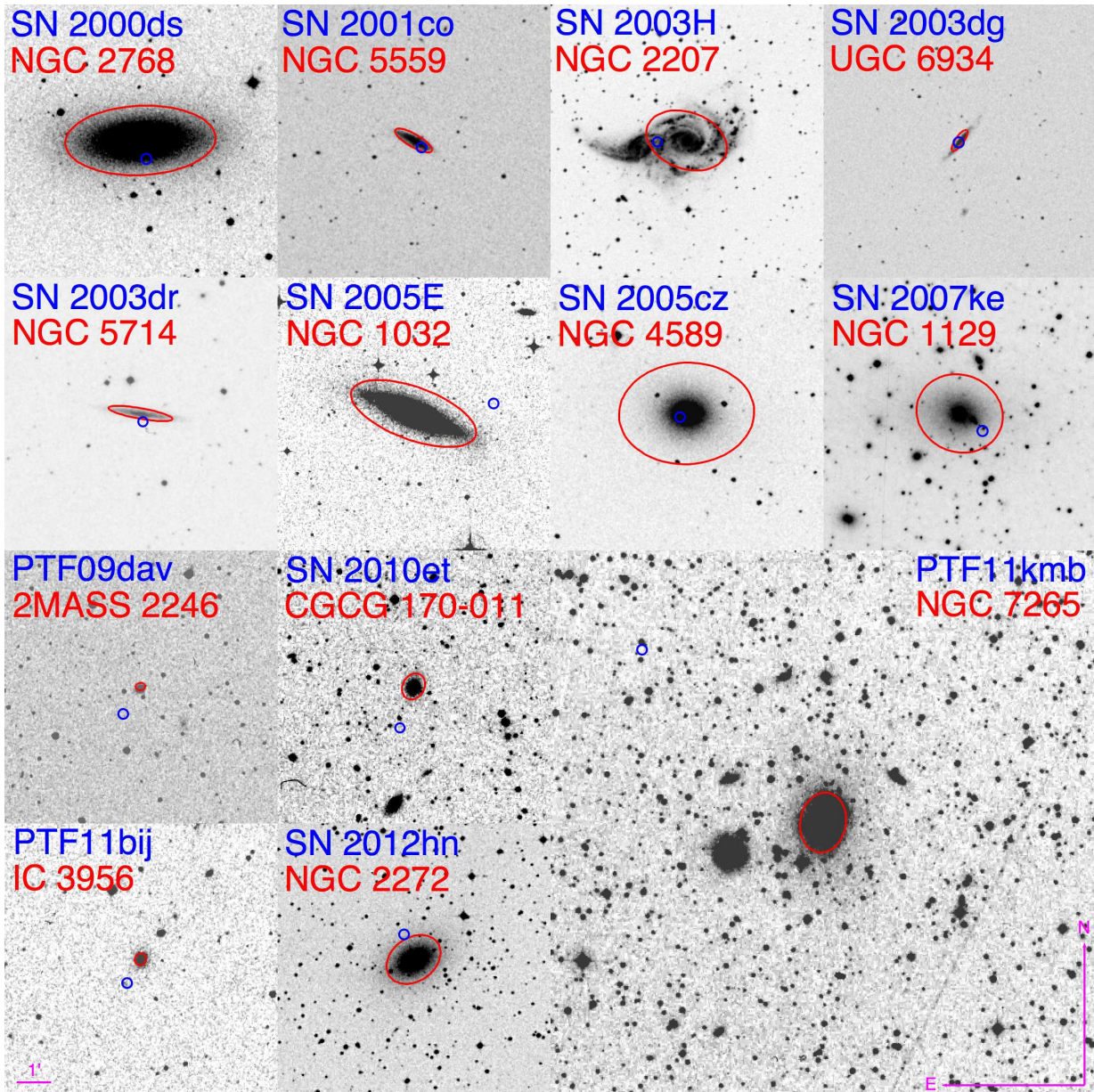


Figure 1. DSS images of Ca-rich SN host galaxies, with each centered in individual panels. Each panel is $8' \times 8'$ except for PTF11kmb, which is $16' \times 16'$. All panels have the same scale and are aligned with North up and East to the left. Each SN position is marked with a blue circle. An ellipse at twice the isophotal radius is shown in red.

and NGC 7265 (offset by 7.3 arcmin, 150.0 kpc, and 10.2 isophotal radii; $cz = 5083 \pm 26 \text{ km s}^{-1}$).

While NGC 7265 is very far physically from PTF11kmb, it is the closest in terms of isophotal radii and has the most similar redshift to that derived from the SN. We therefore adopt NGC 7265 as the host of PTF11kmb for this analysis.

All spectra (except for that of PTF11kmb) were previously published (Kawabata et al. 2010; P10; Sullivan et al. 2011; K12; Valenti et al. 2014). We obtained some of these data through WISERep (Yaron & Gal-Yam 2012).

Almost all SNe in our sample have only one late-time spectrum. For the few SNe with multiple late-time spectra, we primarily analyze the latest high-quality spectrum available. The spectra typically had phases of ~ 2 months after

maximum brightness (e.g., K12). At these phases, and for all spectra examined here, Ca-rich SNe have strong [Ca II] $\lambda\lambda 7291, 7324$ emission, especially relative to that of [O I] $\lambda\lambda 6300, 6363$.

3 HOST-GALAXY PROPERTIES

3.1 Evidence for Recent Host-galaxy Mergers

In Figure 1, we present Digitized Sky Survey (DSS) images of the host galaxies of the Ca-rich SN sample. The host galaxies of Ca-rich SNe are clearly atypical as previously noted (P10; Lyman et al. 2013); the sample is highly skewed to early-type galaxies.

However, previous studies had not noted the strong evidence for recent host-galaxy mergers. In fact, nearly every Ca-rich SN host galaxy shows some indication of a recent merger and/or is in a very dense environment where the likelihood of recent galactic mergers is much larger than in the field.

Of the 13 host galaxies, one is clearly interacting (NGC 2207) and one is a disturbed spiral (2MASS J22465295+2138221; Sullivan et al. 2011). NGC 1129 has a disturbed morphology indicative of a recent merger (Peletier et al. 1990). There are also four S0 galaxies (IC 3956, NGC 1032, NGC 2272, and NGC 7265), which are often thought to be the result of recent mergers (e.g., Moore et al. 1999) or which may have been “harassed” (e.g., Moore et al. 1998). From these tracers alone, 7/13 Ca-rich host galaxies have some indication of a recent merger.

Additionally, at least 8/13 host galaxies are in a group or cluster environment. This is an exceedingly high fraction, even for elliptical galaxies. Moreover, 7/13 host galaxies are either the brightest group galaxy (BGG) or brightest cluster galaxy (BCG). As these galaxies tend to sit at or near the center of the group/cluster potential, they are more likely to have had recent mergers than typical cluster members.

The relative rate of Ca-rich SNe to SNe Ia is roughly 7% (P10). Using the relative fraction of “recent merger” host galaxies for the two groups, the Ca-rich SNe would have a relative rate of only $2 \pm 2\%$ that of SNe Ia in galaxies with no indications of recent mergers and $11 \pm 8\%$ that of the SN Ia rate in galaxies with some indication of a recent merger.

In total, 11/13 Ca-rich SN host galaxies either have some evidence for a ongoing/recent merger or are in dense environments. Using the LOSS SN Ia sample (Leaman et al. 2011), we find that 52% of SN Ia host galaxies have similar host properties. Using binomial statistics, there is only a 1.6% chance that SNe Ia and Ca-rich SNe come from similar host populations in terms of their “recent merger” properties. Since Ca-rich SN and SN Ia host galaxies have indistinguishable morphology and star-formation rate distributions (P10; Lyman et al. 2013), the merger/environment is likely a significant factor in the relative rates. The galaxies in rich environments or that have had recent mergers have an enhanced rate of Ca-rich SNe relative to that of SNe Ia.

3.2 A High Occurrence of AGN

In addition to the different indications of merger activity, several host galaxies also host an active galactic nucleus (AGN). Previously identified AGN include NGC 2207 (Kaufman et al. 2012), NGC 2768 (Véron-Cetty & Véron 2006), NGC 4589 (Ho et al. 1997; Nagar et al. 2005), and IC 3956 (e.g., Liu et al. 2011). Additionally, NGC 1032 has a radio-to-far infrared flux ratio consistent with an AGN (Drake et al. 2003). We also examined the Sloan Digital Sky Survey (SDSS) emission line quantities for the host galaxies observed by SDSS (e.g., Tremonti et al. 2004). For these five galaxies, we identify CGCG 170-011 as a likely AGN, confirm that IC 3956 has a “composite” spectrum indicative of AGN activity, and identify NGC 5559 as having a likely composite spectrum (Figure 2).

At least 6–7 (depending on the classification of NGC 1032) of the 13 Ca-rich host galaxies also host an AGN. This is a large fraction considering that this is an

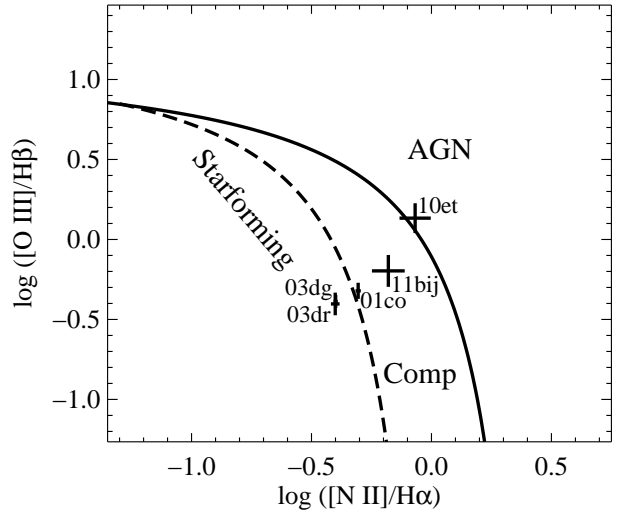


Figure 2. Baldwin-Phillips-Terlevich (BPT) diagram (Baldwin et al. 1981) for the Ca-rich SN host galaxies with SDSS spectra. The curves delineating the star-forming region (below the dashed line), the AGN region (above the solid line) and the “composite” region (between the dashed and solid lines) are taken from Kewley et al. (2001) and Kauffmann et al. (2003) as implemented in Kewley et al. (2006).

incomplete survey of Ca-rich host galaxies. Although the total AGN fraction may be as high as $\sim 43\%$ when the lowest luminosity galaxies and AGN are included (e.g., Ho 2008), this fraction can be lower for specific galaxy samples. For instance, an SDSS spectroscopic sample of $>120,000$ galaxies found that 18% of all galaxies hosted an AGN as determined from line diagnostics (Kauffmann et al. 2003). For the host galaxies with SDSS spectra, 3/5 galaxies also host an AGN. Using binomial statistics for this subsample with the SDSS occurrence rate, there is a 4.7% chance that the Ca-rich host galaxies are typical. If we expand this to the larger, incomplete sample, we find a $<0.4\text{--}2.0\%$ chance (depending on if 6 or 7 galaxies host an AGN). However, we note that if we use a 43% occurrence rate, these differences are not significant for any subsample. For such a rate, $\geq 9/13$ galaxies must host an AGN for a significant difference.

There is likely a connection between the nuclear regions of these galaxies and the SNe offset up to 150 kpc in projection. Since the typical duty cycle of an AGN is $\sim 10^7$ years, the information from the nucleus to SN location would have to travel at a very high speed of $\gtrsim 1000 \text{ km s}^{-1}$.

4 GALACTIC OFFSETS

Ca-rich SNe have been found very far from their host galaxies (e.g., P10; K12). However, this is not exclusively the case. For instance, SN 2003dg was offset $4.1''$ from its host galaxy corresponding to a projected distance of only 1.7 kpc.

Using NED values for the angular size scale and offsets between the SNe and host-galaxy, we determine a projected offset for each SN. The typical uncertainty in the offsets is $\sim 0.1''$, corresponding to projected offset uncertainties of only 0.01 – 0.07 kpc. All SN properties, including those relative to their host galaxies, are presented in Table A2.

In Figure 1, we present Digitized Sky Survey (DSS) images of the host galaxies of the Ca-rich SN sample. In each image, we display an ellipse corresponding to two isophotal radii for each galaxy and the SN position.

To determine the isophotal radial offset for each SN, we use the 2MASS K_s isophotal elliptical parameters (with a reference value of $K_s = 20.0$ mag arcsec $^{-2}$) for each galaxy. For each SN position, we determine a multiplicative factor such that an ellipse with the same axis ratio, position angle, and center will intersect with the SN position. This multiplicative factor is the number of isophotal radii at which the SN is offset.

There are many sources for isophotal parameters, but 2MASS provides a large and homogeneous source. However, these parameters may have somewhat large errors for particular galaxies. The most suspect value is the position angle for NGC 2207. The 2MASS position angle is 70° , while other sources have values of 97° and 141° . It appears that these differences are caused by the different position angles of the bulge/bar and the spiral arms. Nonetheless, NGC 2207 has an axis ratio of 0.68, so the exact angle has only a marginal affect on the measured isophotal radial offset for SN 2003H.

Some galaxies are highly inclined, which is important for understanding the SN offsets. For instance, SN 2003dr is offset only 2.7 kpc (in projection) from its host galaxy nucleus, but it is offset nearly perpendicular to its nearly edge-on host galaxy (minor axis relative to major axis of 0.16). Thus SN 2003dr is offset by 2.9 isophotal radii from the nucleus of its host galaxy.

4.1 Galaxy Targeted SN Search Efficiency

Some Ca-rich SNe have extremely large angular offsets. For instance, SN 2005E and PTF11kmb are offset $2.3'$ and $7.3'$ from their host galaxies, respectively. Galaxy-targeted SN searches, such as LOSS, could potentially miss several Ca-rich SNe because they are offset beyond the field-of-view (FOV) of the camera. This is particularly worrisome since PTF, which runs an untargeted search and has a large FOV camera, has only discovered (and announced) Ca-rich SNe that have a projected distance of at least 34 kpc and up to 150 kpc.

To better understand the efficiency of the LOSS search at finding Ca-rich SNe, we perform a simple calculation. The KAIT camera has a $7.8' \times 7.8'$ FOV. By assuming that a targeted galaxy is centered in the middle of the FOV, we can determine the fraction of projected offsets observed for a galaxy at a given distance.

Figure 3 displays the results from this calculation. For very nearby galaxies, where the scale is 0.1 kpc $''$, KAIT observes 10, 50, and 100% of the area within 83, 37, and 23 kpc, respectively. Since many Ca-rich SNe have peak absolute magnitudes of $M \approx -16$ (P10; K12), KAIT will be magnitude limited for Ca-rich SNe beyond ~ 80 Mpc. At this distance, the scale is ~ 0.4 kpc $''$. For this scale, KAIT observes 10, 50, and 100% of the area within 333, 149, and 93 kpc, respectively. A typical Ca-rich host galaxy within the KAIT sample may have ~ 0.3 kpc $''$, where KAIT observes 10, 50, and 100% of the area within 250, 112, and 70 kpc, respectively.

The farthest offset in the Ca-rich SN sample is PTF11kmb with an offset of 150 kpc. Of the remaining PTF-

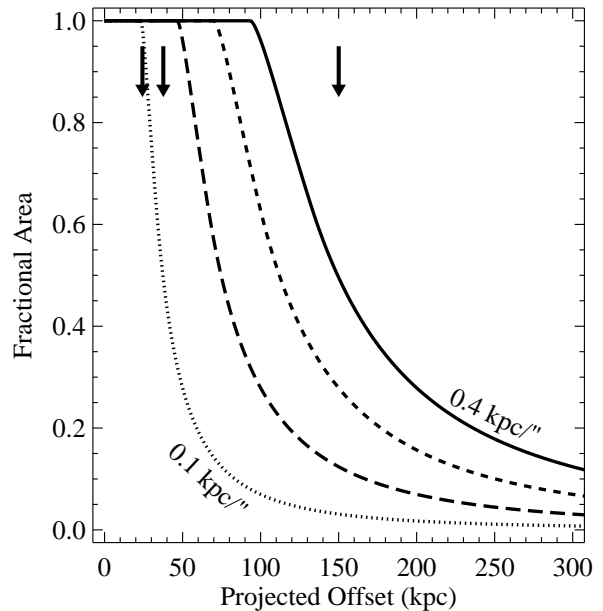


Figure 3. Fraction of the region within a certain projected offset from a particular galaxy observed by KAIT. The dotted, long-dashed, short-dashed, and solid lines correspond to scales of 0.1, 0.2, 0.3, and 0.4 kpc $''$, respectively. The arrows represent, from smaller to larger offsets, the projected offsets of SN 2005E, PTF 11bij, and PTF11kmb, respectively.

discovered Ca-rich SNe, the median offset is 37.6 kpc, and therefore KAIT should have been able to discover such SNe in nearly all of their targeted galaxies. SN 2005E, which was discovered by LOSS (Graham et al. 2005), was offset by 24.3 kpc. In fact, all Ca-rich SNe, with the exception of PTF11kmb, are offset less than $3.9'$, meaning that they would land within the KAIT FOV.

Although KAIT will not be able to discover SNe with extremely large offsets, especially for the closest galaxies, it should be able to sample the bulk of the population discovered by PTF. Although there are likely systematic effects related to humans identifying a transient far offset from a host galaxy as a true SN, there is no technical reason for a lack of Ca-rich SNe with large offsets in the LOSS sample.

Since LOSS is not clearly missing Ca-rich SNe with large offsets, it is reasonable to assume that PTF is missing some Ca-rich SNe with small offsets (or not reporting these objects as Ca-rich SNe). This may be caused by the difficulty of detecting faint sources on top of small galaxies, the difficulty of obtaining high-quality spectra of faint sources on top of relatively bright galaxies, or a preference to obtain multi-epoch, high-quality spectra of SNe Ib with large offsets.

PTF not detecting or not classifying some Ca-rich SNe projected on top of galaxies may also explain the “low” rate for Ca-rich SNe relative to the KAIT rate measurement (P10; K12).

5 VELOCITY SHIFTS

Forbidden lines, which are produced by optically thin material, are extremely useful for understanding the velocity

distribution of SN ejecta along our line of sight. In particular, forbidden emission lines provide the opportunity to measure the bulk velocity offset of the SN ejecta along our line of sight.

For Ca-rich SNe, there are two optical forbidden line complexes which may be studied, [O I] $\lambda\lambda 6300, 6363$ and [Ca II] $\lambda\lambda 7291, 7324$. As a defining property of this class, the SNe have much stronger [Ca II] lines than [O I]. As a result, the majority of our sample has weak or undetectable [O I] lines. However, the [Ca II] lines are sufficiently strong for proper kinematic measurements in all spectra used for this analysis.

5.1 Velocity Measurement Method

For a single emission line, there are three typical measurements used to determine the bulk velocity offset: the peak of emission, the center of a Gaussian fit to the emission profile, and the emission-weighted velocity. If a line profile is Gaussian, the same velocity would be measured from all three methods. However, if there is significant skewness to the profile or multiple peaks, the methods could differ.

For [Ca II] $\lambda\lambda 7291, 7324$ in SN spectra, the doublet is not typically resolved, and this is the case for Ca-rich SNe as well. However, the lines are separated enough such that a single Gaussian is generally not a good description of the data. Moreover, the line profiles are generally moderately skewed, making even the sum of two Gaussian profiles (offset to match the wavelength offset of the doublet) a poor description of the data.

As an example, Figure 4 shows the [Ca II] $\lambda\lambda 7291, 7324$ doublet for SN 2005E. For all line profiles, we subtract the underlying continuum by linearly interpolating across the line profile. The shape of the profile is complicated and far from Gaussian. The profile peaks blueward of the nominal central wavelength with a large drop in emission around zero velocity. Although this has been an indication of dust formation in SN ejecta (e.g., Smith et al. 2008), the long tail of redward emission (extending perhaps 3000 km s^{-1} further to the red than the blue) suggests that the line profile cannot be explained simply by dust reddening. Instead, the profile is likely indicative of a complex velocity structure for the SN ejecta.

Clearly a single Gaussian is not an appropriate description of the [Ca II] profile for SN 2005E. We have also attempted to fit the profile with two Gaussians where their rest-frame wavelength offsets correspond to the difference in wavelengths for the doublets, and their widths and heights are constrained to be the same. These constraints should result in a perfect match to the data if the emitting material were described by a simple velocity distribution. However, SN 2005E has a more complex velocity distribution. Because of the poor Gaussian fits for many spectra in our sample, we do not use this method for our analysis.

A second possibility is to use the peak of emission. Since most spectra contain noise at the level that would affect results (or possibly small scale structure), we smooth the spectra before determining the peak. For SN 2005E, the velocity of the peak of emission is offset from the best-fit Gaussian velocity by 1100 km s^{-1} . The peak of the emission is a particularly poor tracer of the entire SN ejecta since it lacks any information about the shape of the velocity distribution, can

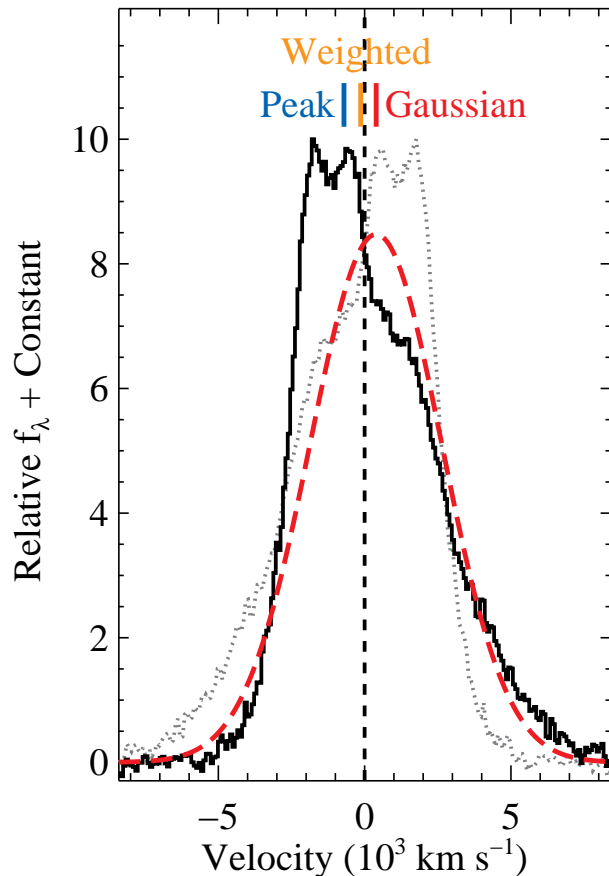


Figure 4. Continuum-subtracted [Ca II] $\lambda\lambda 7291, 7324$ profile for SN 2005E (black curve). The spectrum is also reflected across zero velocity (dotted grey curve) to demonstrate the skewness in the tails of the feature. A best-fit double Gaussian profile with rest wavelengths corresponding to those of the [Ca II] doublet is shown as the red dashed curve. The velocity shifts corresponding to the peak of the smoothed line profile, the emission-weighted center of the profile, and the shift of the double-Gaussian profile are marked with small vertical blue, gold, and red lines.

be influenced by small density perturbations in the ejecta, and is strongly affected by noise in the spectra. We therefore do not use this method of our analysis.

The final possibility is the emission-weighted velocity. Relative to this velocity, half of the emission is blueshifted (and half redshifted). This method uses all information from the line profile, is not affected by the two emission lines, is not significantly affected by noise, and is not affected by skewness. Moreover, this velocity has a specific physical meaning. If the ejecta are completely optically thin and each Ca atom in the ejecta has an equal probability of emitting a photon at these wavelengths, this velocity will correspond to the systemic line-of-sight velocity. As this is clearly the best velocity measurement for determining any line-of-sight velocity shifts, we use this method for our analysis.

5.2 Systematic Uncertainties

While the method chosen to measure of the velocity shift is relatively robust, we investigate possible systematic un-

certainties, which dominate the uncertainty of the velocity measurement.

To determine the uncertainty, we performed a Monte Carlo simulation for each spectrum. For each spectrum, we smoothed the [Ca II] line profile and measured the emission-weighted velocity. Then using noise properties matched to the data, we simulated 1000 spectra for each spectrum. We measured the emission-weighted velocity of each simulated spectrum, randomly changing the regions used to determine the continuum. There was no bias in these measurements, with most shifts from the noise-free spectrum being one or two pixels. This demonstrates the robustness of this method to noisy spectra and with different choices for the continuum. We use the standard deviation of the shifts from the noise-free measurement as the uncertainty in the emission-weighted velocity.

There is an additional potential systematic uncertainty related to the continuum subtraction. Our method assumes a linear underlying continuum. However, if the continuum is dominated by a galaxy spectrum, a linear continuum is not necessarily appropriate. An example of likely host-galaxy contamination for a SN spectrum is shown in Figure 5, where we show the spectrum of SN 2003dg.

We examine the effect of subtracting a galaxy continuum rather than a linear continuum. For this task, we choose an elliptical template spectrum, which appears to be an excellent match to the continuum for SN 2003dg, and a reddened Sc template spectrum since its host galaxy is classified as Scd. Using the elliptical and Sc template spectra result in velocity shifts that are systematically 240 and 80 km s^{-1} bluer than the linear continuum resulting in a velocity shift of -1360 and -1200 km s^{-1} , respectively, compared to our nominal value of -1120 km s^{-1} .

We have examined all spectra, and only two other spectra potentially have host-galaxy contamination. For SN 2001co, the continuum flux is low enough that the choice of continuum does not result in any difference in velocity shift. For SN 2003dr, both the elliptical and Sc templates result in a systematic blueshift of 80 km s^{-1} .

While it is possible that our choice of continuum is biasing the measured velocity shifts for SNe 2003dg and 2003dr, we choose to use the results from having a linear continuum. This choice is conservative given our results (the other choices strengthen our findings). It also provides an easier path to reproducing the methodology with future datasets.

Following the method of P10 (and references therein), we also attempted to subtract a ‘‘photospheric’’ SN continuum from each spectrum assuming that the underlying continuum is caused by photospheric SN emission. We matched our spectra to those of other SNe Ib with similar spectral features away from the nebular lines. We then used these spectra as the underlying continuum. Doing so did not change the measured velocity in any case. For instance, performing the same continuum subtraction used by P10 for SN 2005E, the measured velocity offset shifted by <1 pixel.

This is not surprising given the relative strength of the nebular lines to the continuum. In the case of SN 2005E, which has one of the strongest continua, the continuum is only $\sim 15\%$ the flux of the continuum-subtracted peak [Ca II] flux. Therefore, even 20% changes in the continuum level result in only a $\sim 3\%$ change in the flux at any given wavelength.

Additionally, we examined the consequences of phase on the velocity shift. Unfortunately, only one Ca-rich SN has sufficient data to examine any evolution. SN 2010et has two nebular spectra of reasonable quality that are separated by more than a week. At epochs of roughly 62 and 87 days after peak brightness, we measure a velocity shift of -330 ± 60 and $-430 \pm 60 \text{ km s}^{-1}$, respectively. These measurements differ by only 1.1σ , but may represent a slight velocity gradient of $-4 \pm 3 \text{ km s}^{-1} \text{ day}^{-1}$.

SNe Ia have been shown that their velocity shifts get redder with time (e.g., Silverman et al. 2013), eventually plateauing at a particular velocity as the ejecta become optically thin. While this is a possibility for Ca-rich SNe, we note that SN 2012hn, which has the largest velocity offset and is blueshifted also has one of the latest spectra (+150 days; Valenti et al. 2014).

Currently, there are not enough data to determine the velocity evolution of Ca-rich SNe with phase. Nonetheless, we note that the phase of a SN’s spectrum and its galactic offset are uncorrelated (correlation coefficient of $r = 0.006$), suggesting any potential correlation between offset and velocity is not caused by a correlation between phase and offset.

5.3 Measured Velocity Shifts

In Figure 6, we present the continuum-subtracted [Ca II] $\lambda\lambda 7291, 7324$ profiles for the full Ca-rich SN sample. There is a large diversity to the line profiles with roughly equal numbers having symmetric, skewed blue, and skewed red profiles.

For each spectrum in Figure 6, we mark the emission-weighted velocity. We present these data in Table A1.

For four SNe (2005E, 2010et, PTF09dav, and PTF11bij), K12 measured [Ca II] velocity shifts. Their measurements deviate from ours by -80 km s^{-1} on average, with a median difference of -69 km s^{-1} . The largest difference is for PTF09dav, where we measure a shift of $-110 \pm 60 \text{ km s}^{-1}$, while K12 measure 250 km s^{-1} . While K12 do not describe their method for measuring the velocity shift or list any uncertainties, this represents at most a 5.9σ difference (using only the uncertainty associated with our measurement). All other differences are $<200 \text{ km s}^{-1}$ indicating a general agreement in these measurements.

For 9 Ca-rich SNe, we could also measure an [O I] velocity shift, albeit with much larger uncertainties. Performing a Bayesian Monte-Carlo linear regression on the [Ca II] and [O I] velocity shifts (Kelly 2007), we measure a slope and offset of 0.9 ± 0.9 and 0.2 ± 0.5 , respectively. Therefore, velocity measurements from the [O I] feature are consistent with those of [Ca II], providing additional confidence that the [Ca II] velocity shifts measure any bulk offset to the ejecta.

Five of 13 Ca-rich SNe have absolute velocity shifts of $<300 \text{ km s}^{-1}$ relative to their host galaxy rest frame, which are consistent with coming from galactic motion. However, 8 SNe have larger shifts, up to 1700 km s^{-1} relative to their host galaxy rest frame. Such large velocity shifts must originate from either an asymmetric SN explosion or extreme line-of-sight motion for the progenitor.

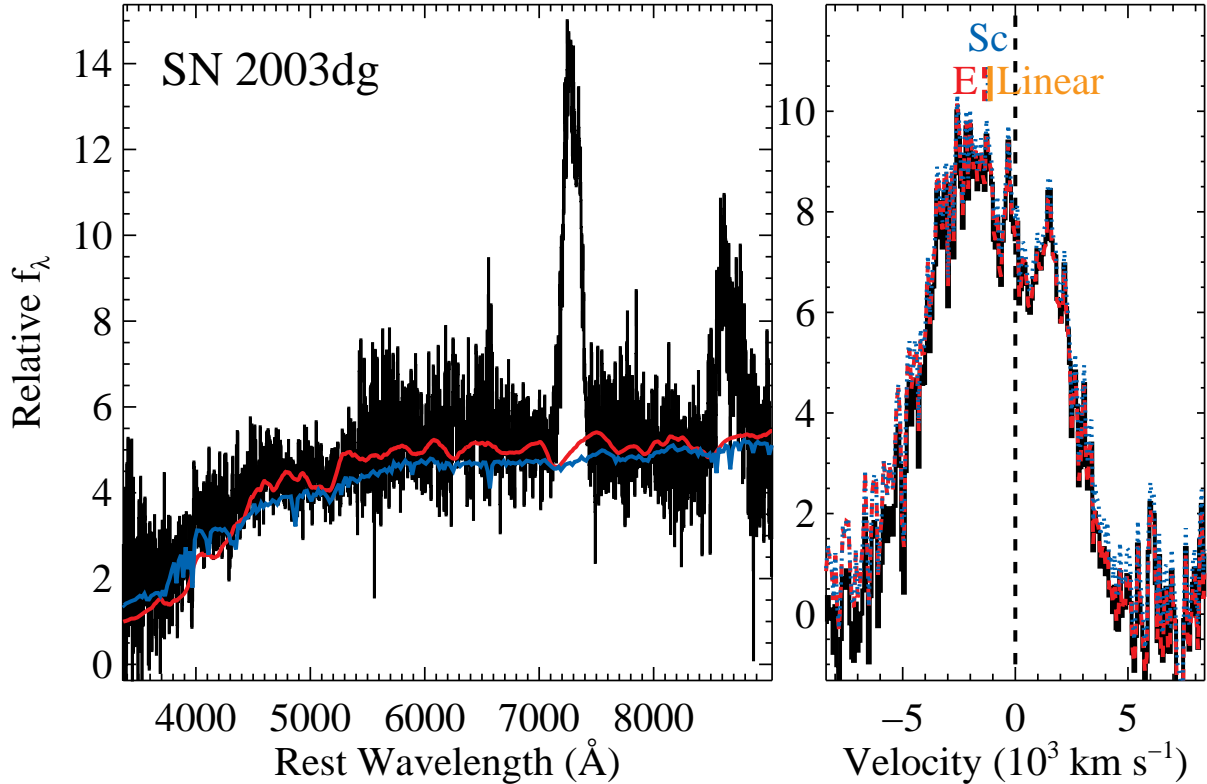


Figure 5. *Left:* Optical spectrum of SN 2003dg (black). Overplotted are template elliptical (red) and reddened ($E(B-V) = 0.35$ mag) Sc (blue) spectra. The galaxy spectra near $[\text{Ca II}] \lambda\lambda 7291, 7324$ is not necessarily linear. *Right:* Corresponding continuum-subtracted $[\text{Ca II}] \lambda\lambda 7291, 7324$ profile for SN 2003dg. The black, red, and blue spectra correspond to a linear continuum, elliptical galaxy, or reddened Sc galaxy subtracted from the SN spectrum. The resulting velocity shifts are plotted above the profile. For this example, the choice of continuum results in a systematic difference in the velocity shift of -240 and -80 km s^{-1} for the elliptical and Sc templates, respectively.

6 ANALYSIS

6.1 The Velocity-Offset Correlation

For the Ca-rich SN sample, there is a large range of velocity shifts (Section 5). However, this range changes with projected offset. SNe with small physical projected offsets have a much larger range of velocity shifts than those with large projected offsets. In particular, within a projected offset of 8 kpc, 4/7 Ca-rich SNe have absolute velocity shifts of $>500 \text{ km s}^{-1}$, while only 1/6 Ca-rich SN beyond 8 kpc has such a large absolute velocity shift (Figure 7).

We also display these data as cumulative distribution functions (CDFs) for Ca-rich SNe within and outside a projected offset of 8 kpc (Figure 8) which also shows the different line-of-sight velocity distributions for these subsamples. To examine the significance of this difference, we employ the Anderson-Darling statistical test. The Anderson-Darling test is similar to the Komogorov-Smirnov test except it is more sensitive to differences in the tails of distributions. Such a test is particularly useful for this analysis since we would naively expect any velocity shift distribution to be centered at roughly zero velocity and differences to be in the tails of the distributions. If the distributions are normal, the Anderson-Darling test reduces to the Komogorov-Smirnov test.

The Anderson-Darling statistic for these two subsamples results in a p -value of 0.031, indicating that the Ca-rich

SNe with small and large projected offsets are drawn from parent populations with different velocity shifts. This distinction is relatively insensitive to the exact distance used to separate the subsamples. Any chosen separation ranging from 7.1 – 16.7 kpc produces significantly different subsamples.

We also note that while we may be systematically missing Ca-rich SNe near the centers of their host galaxies with redshifted velocity shifts (Section 4.1), the inclusion of these SNe, if they have a similarly extreme velocity distribution as those with blueshifted velocity shifts, would only make the tails of the distributions more discrepant and difference between the subsamples more significant.

This result is incredibly indicative. First, if the velocity shifts were primarily caused by the explosion or a binary orbital velocity, there should be no correlation with projected offset. Therefore, the velocity shifts are almost certainly the result of extreme line-of-sight motion for the progenitor. To account for the SNe with extreme velocity offsets, some progenitor systems must be given a velocity kick of $\gtrsim 1500 \text{ km s}^{-1}$.

There is an additional clue which indicates that the velocity shifts are not caused by the explosion. Velocity shifts are seen in SNe Ia (e.g., Maeda et al. 2010) and those shifts are thought to be a bulk offset of the core of the ejecta relative to the outer layers. However, SN Ia explosions appear to be constrained to have relatively small velocity shifts com-

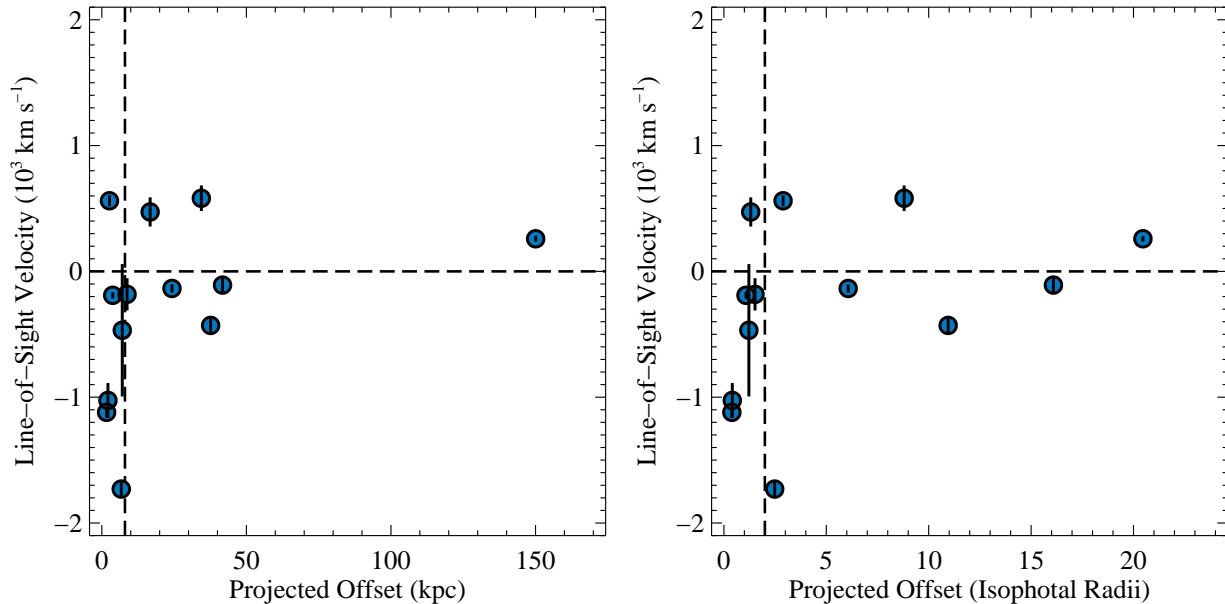


Figure 7. Line-of-sight velocity shifts as a function of projected offset (*left*) and isophotal radial offset (*right*) for the Ca-rich sample. Velocity uncertainties are typically smaller than the data points. Only 4/13 SNe have a redshift, while only 1/6 SNe within two isophotal radii (and 8 kpc) have a redshift and 3/7 outside two isophotal radii (and 8 kpc) have redshifts.

pared to the full-width at half-maximum (FWHM) of their emission lines. Using a sample of 22 SNe Ia (Blondin et al. 2012), we find that the most extreme velocity shifts are $<20\%$ that of their FWHM. For the Ca-rich SN sample, 3/13 have more extreme velocity shifts (relative to FWHM) than any SN Ia in the Blondin et al. (2012) sample.

Figure 9 shows the CDFs of velocity shifts relative to FWHMs for the Ca-rich and SN Ia samples. The Anderson-Darling statistic for these two subsamples results in a p -value of 0.040, indicating that these samples are drawn from different parent populations. This result implies that either Ca-rich SNe come from significantly more asymmetric explosions than SNe Ia or there is an additional line-of-sight velocity component for some Ca-rich SNe. The latter is consistent with a correlation between velocity shift and projected offset.

The velocity-offset correlation further indicates that the line-of-sight motion for the progenitor must be correlated with the projected offset. The most obvious explanation is that most progenitor systems originate near the centers of their host galaxies, are given a large kick, and when they ultimately explode, have the velocity kick imprinted in the kinematics of the ejecta. For a progenitor that travels along our line of sight, there will be no projected offset for the SN, but its line-of-sight velocity offset will be large. Meanwhile, for a progenitor that travels perpendicular to our line of sight, the SN will have a large projected offset but a velocity offset close to zero (although the SN explosion or orbital motion of the progenitor system, as well as measurement errors may result in some velocity offset).

Therefore, Ca-rich SNe progenitor systems do *not* typically originate from globular clusters, in-falling dwarf galaxies, the intracluster medium, or other large-offset components of a galaxy.

From the velocity-offset data alone, it is possible that

Ca-rich SN progenitor systems originate in the disk or halo, offset from the galaxy’s nucleus, and (in some cases) are kicked to large offsets.

6.2 An Excess of Blueshifts

The velocity offset distribution for the Ca-rich SN sample is skewed to the blue. Nine of the 13 SNe are blueshifted, while the remaining 4 are redshifted. This is particularly striking when examining the 6 SNe within two isophotal radii of their host galaxies (Figure 7). Only a single SN in this subsample is redshifted. However, 3/7 of the Ca-rich SNe with larger offsets are redshifted. The likelihood of having such skewed distributions are only 17.5% and 18.8% for the full sample and small-offset subsample, respectively. This calculation accounts for the possibility that the distribution could be skewed in the opposite direction as well (if only considering blueshifts, the likelihood is half of that reported above).

Although this is not a statistically significant result, it is noteworthy because of a physically motivated reason for such a difference. If the progenitor systems were kicked from the centers of their galaxies with velocities larger than the escape velocity of the galaxy, then the velocity shift will be blueshifted for SNe on the near side of the galaxy. In such a scenario, redshifted SNe will be on the far side of their host galaxies, and therefore will be more likely to suffer from dust extinction. Thus, Ca-rich SNe with redshifted velocity shifts will be harder to detect, resulting in under-representation in the full sample.

This is further support for most Ca-rich SN progenitors originating from near the centers of their host galaxies. If their progenitors came from bound orbits (such as from a globular cluster population), there should be an equal number of blueshifted and redshifted SNe on the near side of the

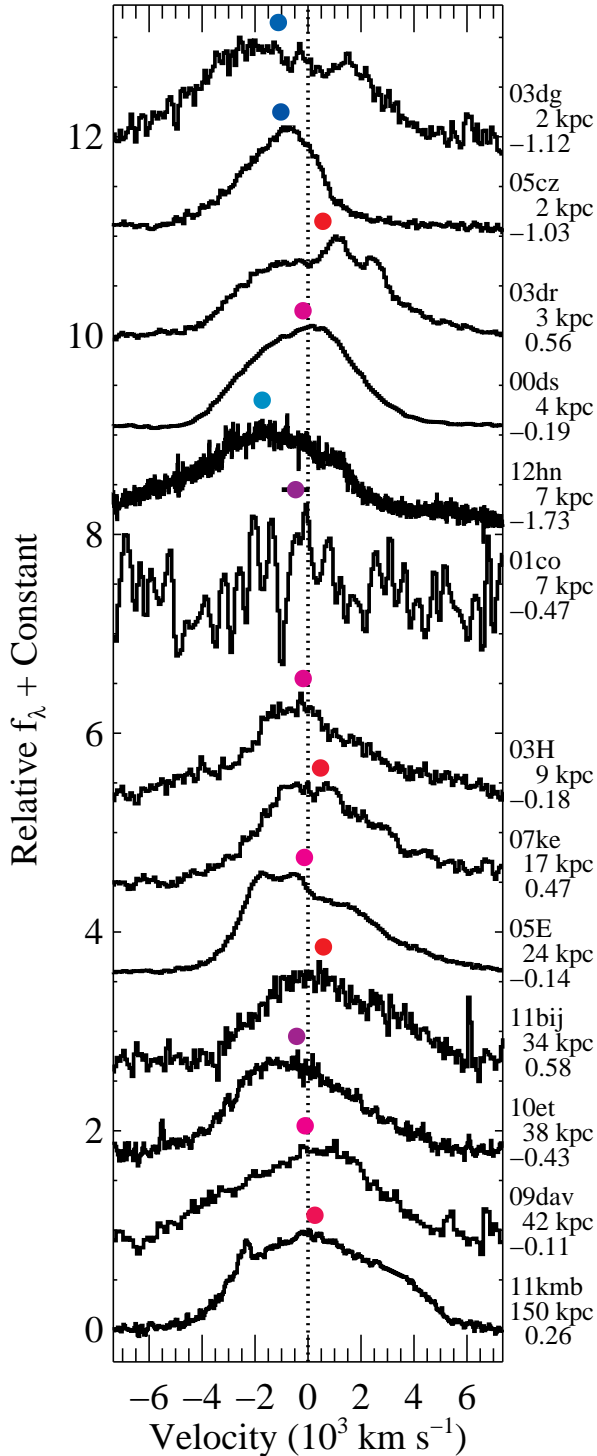


Figure 6. Continuum-subtracted [Ca II] $\lambda\lambda 7291, 7324$ profiles of the Ca-rich SN sample on a velocity scale relative to the host-galaxy frame. The spectra are ordered by physical projected offset. A circle indicates the emission-weighted velocity of each feature. The uncertainty for each velocity measure is plotted, however, most uncertainties are smaller than the plotted symbols. The offset and velocity (in 10^3 km s^{-1}) are listed next to each spectrum.

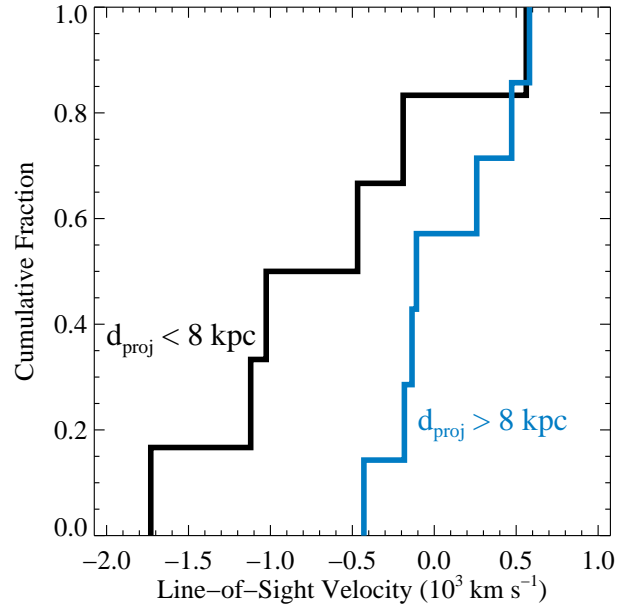


Figure 8. Line-of-sight velocity shift CDFs for the Ca-rich SNe with a projected offset $< 8 \text{ kpc}$ (black line) and $> 8 \text{ kpc}$ (blue line). The SNe with small projected offsets have a wider distribution of line-of-sight velocity shifts ($p = 0.031$).

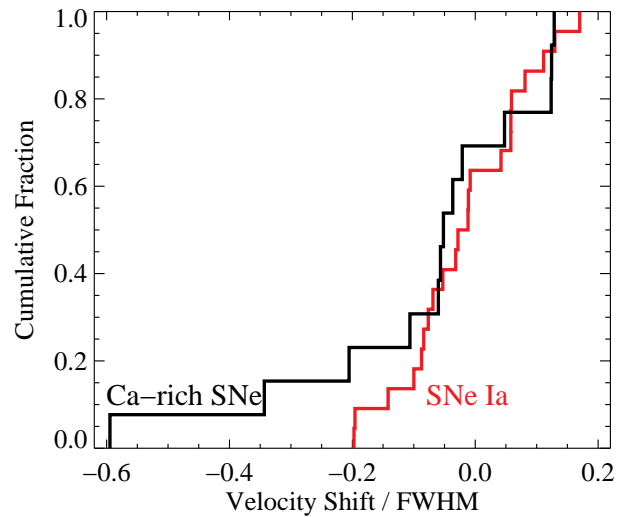


Figure 9. CDFs of velocity shifts relative to nebular line FWHMs for the Ca-rich (black) and SN Ia (red) samples. Some Ca-rich SNe have much larger velocity shifts relative to the widths of their lines compared to the SN Ia sample. This indicates an additional velocity component. The Anderson-Darling statistic for these two subsamples results in a p -value of 0.040.

galaxy, and therefore no noticeable difference in the observed population. Furthermore, for progenitors in-falling towards the host galaxy for the first time, we would expect more *redshifted* SNe, the opposite of what is observed.

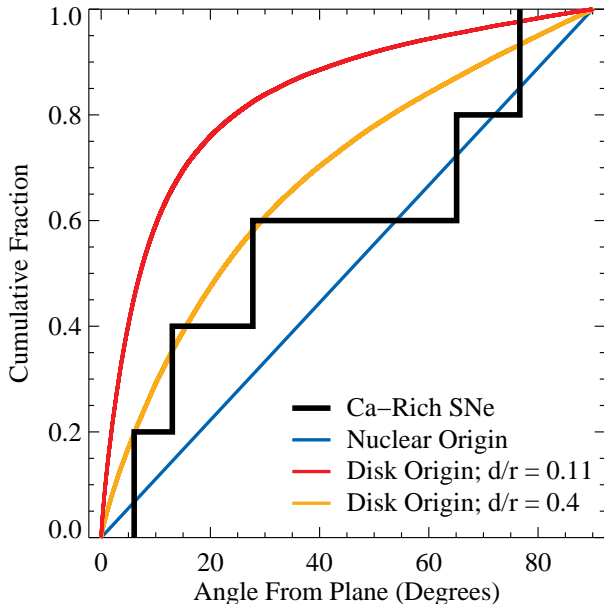


Figure 10. Offset-angle CDF for Ca-rich SNe in edge-on galaxies (black). Also shown are theoretical distributions corresponding to a nuclear origin (blue line), a disk origin with the distance traveled by the progenitor system, d , relative to the major axis of the disk, r , of 0.11 or 0.4 (d/r ; red and gold curves, respectively). The disk origin with $d/r = 0.11$ is inconsistent with the observed distribution, while larger offsets relative to the height or the nuclear origin are consistent with the data.

6.3 The Offset Angle Distribution

A final observational indication of the origin of Ca-rich SNe from the SNe themselves is the angle between the SN and the disk of the galaxy, which we call the offset angle. A non-disk origin should have a flat offset angle distribution (all angles are equally likely). However, a disk origin will tend to have more SNe with small angles relative to the disk. The exact offset angle distribution for the disk depends on the average distance traveled by the progenitor system, d , relative to the major axis of the disk, r . For example, if $d/r = 0$, corresponding to the SNe exploding in the disk, then all offset angles would be zero. A larger value of d/r means that SNe will be further above the disk (on average) and thus the offset angle distribution will be flatter.

In Figure 10, we plot the offset angle distribution for the Ca-rich SNe with close to edge-on disks (axis ratios of <0.5). This corresponds to 5 SNe: SNe 2000ds, 2001co, 2003dg, 2003dr, and 2005E. Of these 5, SNe 2000ds and 2003dr have offset angles $>65^\circ$. The observed distribution is consistent with a flat distribution.

To generate the theoretical disk distributions, we assumed an infinitely thin exponential disk perfectly edge on. For this stellar distribution, we chose random angles in three dimensions, and offset an amount d along those angles. We then measured the offset angle to the SN site. As expected, a smaller value of d/r results in a distribution more peaked to zero degrees.

We use the Anderson-Darling statistic to determine what values of d/r are consistent with the data. Ca-rich

SNe are inconsistent with coming from a disk population with ratios of $d/r \leq 0.11$.

We cannot know the value of d for our SNe, however, we can measure the distance the SNe are above the disk, z , which must be a lower limit on d . For the edge-on subsample, there is a range of $0.04 \leq z/r \leq 0.56$. Therefore, a value of $d/r \approx 0.4$ may be appropriate, making a disk origin consistent with the observed angle offset distribution.

More observations should further constrain any possible disk contribution.

7 A BASIC MODEL

Previous studies have shown that Ca-rich SNe have He in their ejecta (e.g., Kawabata et al. 2010; P10) and come from older stellar populations (e.g., P10). These observations suggest an old progenitor system, and a massive-star progenitor is unlikely. The most obvious long-lived progenitor system with a large abundance of helium is one that contains a He WD or a hybrid He-C/O WD. As these stars are not expected to explode in isolation, a favorable progenitor system is a He-C/O WD binary system. Simulations suggest that a merger (or surface detonation after mass transfer) for these systems can broadly reproduce the Ca-rich SN properties (e.g., Kromer et al. 2010; Shen et al. 2010; Waldman et al. 2011; Sim et al. 2012; Dessart & Hillier 2015).

Ca-rich SNe have an extended projected offset distribution (e.g., K12). While some have attempted to explain this as Ca-rich SNe having dwarf galaxy, globular cluster, and/or intracluster origins, these scenarios are inconsistent with other data. For instance, if there is a dwarf galaxy origin, there should not be such a strong correlation with nearby early-type galaxies.

The strongest evidence against these previous scenarios is that there is no indication of any stellar population at the position of any Ca-rich SN to quite deep limits (P10; Perets et al. 2011; K12; Lyman et al. 2013, 2014). This last observation requires that the progenitors of Ca-rich SNe be born far from where they explode (Lyman et al. 2014).

Our kinematic data indicates that the progenitors of Ca-rich SNe originate near the centers of their galaxies. There is a strong correlation between the line-of-sight velocity shifts and projected offsets for the Ca-rich SN sample (Section 6.1). The measured velocity shifts for some SNe is much larger than typical stellar velocities and even larger than the escape velocity of a galaxy (Section 5). In fact, the line-of-sight velocities of several Ca-rich SNe is larger than the expected maximum velocity from a disk origin ($\sim 1000 \text{ km s}^{-1}$; e.g., Tauris 2015), but is consistent with that of Galactic hyper-velocity stars (HVSs; Brown et al. 2014; Palladino et al. 2014). From kinematic data alone, it is most likely that Ca-rich progenitor systems have been kicked after an interaction with a supermassive black hole (SMBH) at the center of their host galaxies.

We have shown that almost all Ca-rich SN host galaxies are merging, have recently merged, have characteristics indicative of a recent merger, and/or are in dense environments where the probability of a merger is high (Section 3.1). A binary SMBH can easily fill its loss cone, and therefore the HVS ejection rate of such systems are enhanced by a

factor of $\sim 10^4$ (Yu & Tremaine 2003) over those of single SMBHs (e.g., Hills 1988).

The ejection rate of hyper-velocity binary stars (HVBSs) is expected to be exceedingly low for single SMBHs, but perhaps half of all binary stars interacting with a binary SMBH are ejected at hyper velocities with the binary intact (Lu et al. 2007; Sesana et al. 2009). This mechanism is also expected to change the orbital properties of the binary. In particular, eccentricities of 0.9 – 1 can be excited in these systems (Lu et al. 2007). Presumably, such orbits will again circularize, but in doing so, significantly reduce their separation.

If a close encounter with a SMBH is necessary to produce a Ca-rich SN progenitor system or to significantly reduce its delay time, a recent galaxy merger should also significantly enhance the Ca-rich SN rate. In retrospect, one might have been able to predict that Ca-rich SNe should be preferentially hosted by galaxies that have undergone recent mergers.

Additionally, we have shown that a large fraction of Ca-rich SN host galaxies also host an AGN (Section 3.2). After a merger, it is expected that many SMBHs will have their gas supplies replenished, and such galaxies will host an AGN. However, such activity can be relatively short-lived. The typical duty cycle of an AGN is $\sim 4 \times 10^7$ years. Because AGN activity is relatively short-lived, any correlation between Ca-rich SNe and AGN activity suggests a physical connection. If one simply wants information to be transferred between the nucleus and SN location, that information must travel at a speed of $\gtrsim 750 \text{ km s}^{-1}$ for a separation of 30 kpc (similar to the separation between PTF11bij and the AGN in its host galaxy, 34 kpc). Notably, this velocity is larger than typical SN kicks. However, the expected hyper-velocity kicks from a SMBH interaction is typically, $\sim 1500 \text{ km s}^{-1}$, larger than, but within a factor of 2 of, the minimum speed for information travel in some Ca-rich galactic systems.

With these strong pieces of evidence (helium in the system, an old stellar population, a lack of a stellar population at the position of the SNe, a correlation between line-of-sight velocity shifts and projected offset, a significant number of host galaxies with a high-likelihood of recent mergers, and a high AGN fraction for the host galaxies), we suggest a possible progenitor system for Ca-rich SNe: a He-C/O WD binary system that has recently been ejected from its host galaxy after an encounter with a SMBH. The ejection rate will be significantly enhanced in galaxies with a binary SMBH, and therefore also in galaxies which have recently undergone a merger. Although it is possible for a Ca-rich SN to occur without an encounter with a SMBH, this must not be the dominant progenitor path for Ca-rich SNe. If Ca-rich SNe commonly came from systems that did not interact with a SMBH, we would not see the strong connections to mergers, AGN activity, or even the large offsets. Instead, the interaction with the SMBH must significantly enhance the SN rate, likely by significantly decreasing the delay time (perhaps from a typical delay time of greater than a Hubble time to one similar to the AGN duty cycle).

7.1 Additional Model Constraints

Such a progenitor model has other observational consequences consistent with current data. For instance, we would

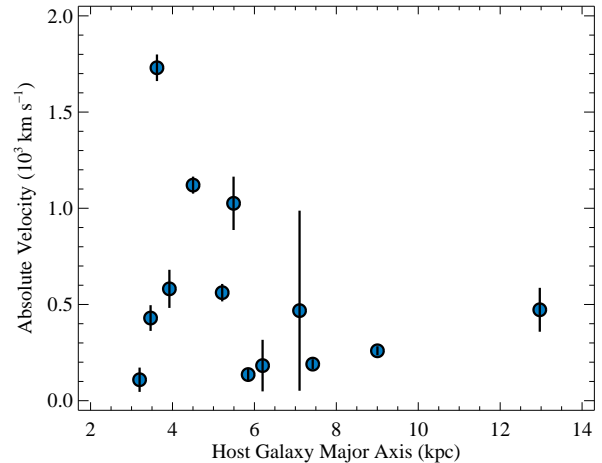


Figure 11. Magnitude of velocity shifts as a function of host-galaxy size (as measured by the major axis) for the Ca-rich sample.

expect a flat offset angle distribution. Such a distribution is consistent with our observations (Section 6.3). Additionally, as the SNe would be on unbound orbits, the SNe projected on top of their galaxies would have the highest velocity shifts. However, if there is dust reddening in the galaxy, we would expect redshifted SNe to be more difficult to detect, resulting in an excess of SNe with blueshifted velocity shifts. Such an excess has also been observed (Section 6.2).

A final testable prediction of our model is that there should be an anti-correlation between the magnitude of the velocity shift and the size of the galaxy. Larger galaxies with larger gravitational potential wells should reduce the velocity shift more than smaller galaxies. Alternatively, if the SN progenitors originated in satellite galaxies or globular clusters, the SN systemic velocity relative to their host galaxy should increase with increasing host-galaxy mass.

Figure 11 shows the magnitude of the velocity shifts as a function of host galaxy size for our sample. There is an obvious anti-correlation with the highest-velocity SNe coming from the most compact galaxies. While this is not a strong correlation ($r = -0.29$), the size of a galaxy is not a perfect proxy for gravitational potential, and cluster environments must further augment that potential, this is further observational support for our model and evidence against a dwarf galaxy or globular cluster origin.

7.2 Model Implications and Predictions

Our model requires that the inherent Ca-rich SN rate be extremely low and an encounter with a SMBH must somehow substantially increase the rate. This is perhaps through changing the orbital dynamics of the system or by triggering a physical change in a star in the system. There is a clear example of the former possibility. If the typical progenitor system is a binary system with a separation large enough such that a merger through gravitational radiation is longer than a Hubble time, then the inherent Ca-rich SN rate will be necessarily low. However, an interaction with a SMBH (perhaps preceded with other interactions in the

nuclear star cluster) could then reduce the merger time to significantly less than a Hubble time.

We can estimate the post-kick merger time for these systems. If we assume that a typical kick velocity is 1000 km s^{-1} , a star system would have traveled for 30 or 150 Myr to travel 30 or 150 kpc, respectively. While it is possible that some kicks result in bound orbits or that some SNe with large projected offsets also have relatively large line-of-sight offsets, these scenarios cannot be a significant portion of the population. Therefore, in our model, the typical post-kick delay time is about 10–100 Myr. This timescale is similar to that of the AGN duty cycle.

However, if this delay time is equivalent to a binary merger time, it must require a change in orbital separation by a factor of 10–100. This requirement may be reduced some if the binary is initially hardened by interactions in the nuclear star cluster. If this is the case, we would expect many more Ca-rich SNe in galactic nuclei. Although there are known systematics for detecting nuclear SNe, the lack of a substantial population of nuclear events in the current sample is a hurdle for such an explanation.

Detailed calculations of the orbital parameters of potential progenitor systems after ejection are required to measure a change in final separation and merger time.

Another implication of the model is the relative rate of Ca-rich SNe in galaxies with and without recent mergers. Assuming that the progenitor systems are formed before a merger and all galaxies have a similar number of progenitor systems near their SMBHs, the relative Ca-rich SN rate per unit mass should be equivalent to the relative ejection rate, or $\sim 10^4$. Since the ratio of recent mergers to non-merging systems is roughly 10^{-2} , the observed relative rate should be $\sim 10^2$. That is, for every Ca-rich SN in a non-merging system, there should be 100 Ca-rich SNe in merging systems. The current Ca-rich sample appears to have $\sim 1/13$ non-merging systems is consistent with this estimate. However, this estimate is only approximate and could be off by an order of magnitude. Similarly, the current sample may be highly biased or we may have incorrectly estimated the number of merging systems. This question should be revisited with more detailed calculations and a larger SN sample.

Nonetheless, the relative rate of Ca-rich SNe to SNe Ia has been measured to be $\sim 5\%$. If we assume that Ca-rich SNe occur exclusively in merging systems, the Ca-rich SN rate must be ~ 5 times that of the SN Ia rate in these galaxies. The SN Ia rate in S0 galaxies is roughly 0.1 SNe Ia per century (Li et al. 2011) or $10^{-3} \text{ year}^{-1}$. A $6.5 \times 10^6 M_{\odot}$ SMBH with a full loss cone has an ejection rate of ~ 2 stars per year. Therefore, Ca-rich SN progenitor systems must represent $\sim 0.25\%$ of all ejected systems in these galaxies. Considering the potentially high survival rate of compact binary systems with binary SMBHs (Lu et al. 2007), this order-of-magnitude calculation appears to have the Ca-rich SN rate compatible with the ejection rate.

8 DISCUSSION AND CONCLUSIONS

Ca-rich SNe are rare and peculiar low-luminosity Type I SNe with He in their spectra near maximum brightness and relatively strong Ca emission at late times. While many of these SNe are within one isophotal radius of their host galaxies, a

significant percentage occur far from their host galaxies — some farther than any other detected SN.

The Ca-rich SNe with small projected offsets tend to have much larger line-of-sight velocity shifts as determined from the emission-weighted velocity of forbidden lines. The correlation between projected offset and line-of-sight velocity shifts indicates that the progenitors of Ca-rich SNe have been kicked from near the centers of their galaxies.

The highest velocity shifts are too large for a disk origin, but are consistent with a kick from an interaction with a SMBH. A nuclear origin is further supported by a slight excess of blueshifted velocity shifts with small offsets, an offset angle distribution consistent with isotropic kicks from a galactic nucleus, and an anti-correlation between the magnitude of the line-of-sight velocity shifts and galaxy size.

The host galaxy population has a significant number of merging/disturbed galaxies, S0 galaxies, and brightest cluster/group galaxies — all of which are more likely to have had recent mergers than typical galaxies. Such an observation must be linked to the prevalence of Ca-rich SN progenitor systems. A recent galaxy merger enhancing the interaction rate between Ca-rich SN progenitor systems and a SMBH is one possible reason for this observation. Such a scenario is expected to boost the SMBH ejection rate by a factor of $\sim 10^4$, making observed and theoretical rates broadly consistent.

The fraction of Ca-rich SN host galaxies with AGN is high. The AGN fraction is yet another indication of recent mergers. The timescale for AGN activity also places a soft upper limit on the delay time since galaxy merger of $\sim 4 \times 10^7$ years and an independent lower limit on the velocity of ejected systems.

The host-galaxy morphology distribution is indicative of an older progenitor population (P10). The He in the early-time spectra of Ca-rich SNe suggests a significant amount of He is in the progenitor system. As the progenitor system is likely old, the source is likely a He WD.

As a possible progenitor hypothesis, we propose the following: the progenitor system for a Ca-rich SN is a binary system consisting of a He WD with a C/O WD. This system must have a typical merger time longer than a Hubble time, which is most likely achieved with a low-mass double WD system. This system is kicked to high velocity after interaction with a SMBH in the center of its host galaxy. During this interaction, the binary is significantly hardened such that the delay time is reduced to ~ 50 Myr. Such a possibility seems plausible for binary systems ejected after interacting with a binary SMBH, which is also expected to significantly reduce the merger time (Lu et al. 2007). After traveling, on average, several to tens of kpc, the system merges and results in a Ca-rich SN.

P10 examined the possibility of the progenitor of SN 2005E being ejected as a HVS, however they only examined this for a potential high-mass ($M > 8M_{\odot}$) progenitor. They found that such a progenitor system was unlikely, but did not address the possibility of a low-mass binary progenitor ejected at hyper velocity.

If this scenario is correct, the progenitor systems of Ca-rich SNe represent the first indication of extragalactic HVSs and the first detection of HVBSs ejected from a galactic center. These peculiar SNe would provide the best way to observe HVSs beyond the local group. Ca-rich SNe may be

an excellent tracer of the SMBH population in general and binary SMBHs in particular. Ca-rich SN host galaxies may provide an excellent input catalog for future binary SMBH studies. Moreover, the Ca-rich SN rate may be an indirect tracer of the galaxy merger rate.

We caution that the details of our toy model are currently poorly constrained. The current sample size is small and likely biased against nuclear events (and perhaps against SNe with the largest projected offsets). An order of magnitude larger sample, which can be achieved in the next few years with upcoming surveys combined with dedicated spectroscopic resources, will provide necessary kinematic constraints to infer the underlying properties of the Ca-rich SN progenitor population.

ACKNOWLEDGMENTS

Facility: Keck I(LRIS)

R.J.F. is incredibly thankful for extended discussions on this work with P. Behroozi, and J. Guillochon, and E. Ramirez-Ruiz. We also thank L. Bildsten, R. Chornock, A. Filippenko, D. Kasen, K. Mandel, H. Perets, and K. Shen for discussing Ca-rich SNe and providing insights on this work over the past several years.

We thank the participants of the “Fast and Furious: Understanding Exotic Astrophysical Transients” workshop at the Aspen Center for Physics, which is supported in part by the NSF under grant No. PHYS-1066293. Multiple discussions at the workshop motivated portions of this work. R.J.F. also thanks the Aspen Center for Physics for its hospitality during the “Fast and Furious” workshop in June 2014.

The Digitized Sky Surveys (DSS) were produced at the Space Telescope Science Institute under U.S. Government grant NAG W-2166. The images of these surveys are based on photographic data obtained using the Oschin Schmidt Telescope on Palomar Mountain and the UK Schmidt Telescope. The plates were processed into the present compressed digital form with the permission of these institutions.

This research has made extensive use of the NASA/IPAC Extragalactic Database (NED) which is operated by the Jet Propulsion Laboratory, California Institute of Technology, under contract with the National Aeronautics and Space Administration.

This research has made use of the Keck Observatory Archive (KOA), which is operated by the W. M. Keck Observatory and the NASA Exoplanet Science Institute (NExScI), under contract with the National Aeronautics and Space Administration.

APPENDIX A: OBSERVATIONS OF PTF11kmb

PTF11kmb was discovered PTF on 24.24 August 2011 and was spectroscopically classified as a SN Ib from a spectrum obtained on 28 August 2011 (Gal-Yam et al. 2011).

PTF11kmb was observed on 28.52 August 2011 (PI Filippenko; Program U048LA) and 26.37 November 2011 (PI

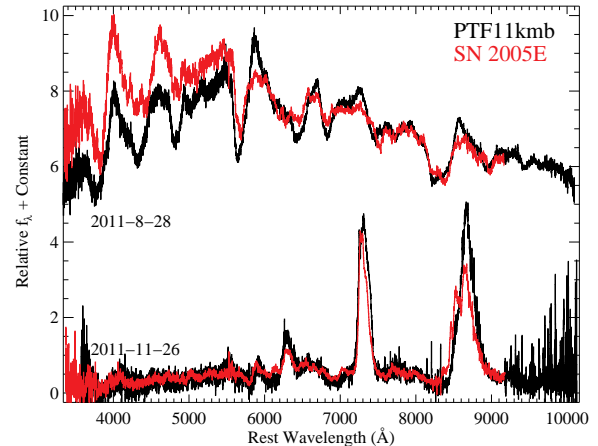


Figure A12. Optical spectra of PTF11kmb (black curves) from 28 August 2011 (top) and 26.37 November 2011 (bottom). Comparison spectra of SN 2005E from 15.35 January 2005 (top) and 11.26 March 2005 (bottom; P10) are displayed in red. All spectra have been corrected for Milky Way reddening. The continuum is slightly different at early times, but this is likely the result of being at somewhat different phases or having different temperatures.

Kulkarni; Program C219LA) with the Low Resolution Imaging Spectrometer (LRIS; Oke et al. 1995) mounted on the Keck I telescope. The August spectrum had a 450 s integration, while the November spectrum had 1200 s blue-channel and 2×570 s red-channel integrations. The August spectrum was originally used to classify PTF11kmb as a SN Ib.

We obtained these data through the Keck Observatory Archive. Standard CCD processing and spectrum extraction were accomplished with IRAF¹. The data were extracted using the optimal algorithm of Horne (1986). Low-order polynomial fits to calibration-lamp spectra were used to establish the wavelength scale, and small adjustments derived from night-sky lines in the object frames were applied. We employed our own IDL routines to flux calibrate the data and remove telluric lines using the well-exposed continua of spectrophotometric standards (Wade & Horne 1988; Foley et al. 2003; Silverman et al. 2012). The spectra are presented in Figure A12.

As the comparisons to SN 2005E in Figure A12 show, PTF11kmb is clearly a member of the Ca-rich class of SNe.

REFERENCES

- Baldwin J. A., Phillips M. M., Terlevich R., 1981, *PASP*, 93, 5
- Berger E., Fong W., Chornock R., 2013, *ApJ*, 774, L23
- Blondin S. et al., 2012, *AJ*, 143, 126
- Brown W. R., Geller M. J., Kenyon S. J., 2014, *ApJ*, 787, 89
- Dessart L., Hillier D. J., 2015, *MNRAS*, 447, 1370

¹ IRAF: the Image Reduction and Analysis Facility is distributed by the National Optical Astronomy Observatory, which is operated by the Association of Universities for Research in Astronomy, Inc. (AURA) under cooperative agreement with the National Science Foundation (NSF).

- Drake C. L., McGregor P. J., Dopita M. A., van Breugel W. J. M., 2003, *AJ*, 126, 2237
- Filippenko A. V., Chornock R., Swift B., Modjaz M., Simcoe R., Rauch M., 2003, *IAU Circ.*, 8159, 2
- Filippenko A. V., Li W. D., Treffers R. R., Modjaz M., 2001, in *ASP Conf. Ser.* 246: *IAU Colloq. 183: Small Telescope Astronomy on Global Scales*, Paczynski B., Chen W.-P., Lemme C., eds., pp. 121–+
- Foley R. J. et al., 2013, *ApJ*, 767, 57
- Foley R. J., Narayan G., Challis P. J., Filippenko A. V., Kirshner R. P., Silverman J. M., Steele T. N., 2010, *ApJ*, 708, 1748
- Foley R. J. et al., 2003, *PASP*, 115, 1220
- Gal-Yam A. et al., 2011, *The Astronomer's Telegram*, 3631, 1
- Graham J., Li W., Schwartz M., Trondal O., 2005, *IAU Circ.*, 8465, 1
- Hills J. G., 1988, *Nature*, 331, 687
- Ho L. C., 2008, *ARA&A*, 46, 475
- Ho L. C., Filippenko A. V., Sargent W. L. W., 1997, *ApJS*, 112, 315
- Horne K., 1986, *PASP*, 98, 609
- Kasliwal M. M. et al., 2012, *ApJ*, 755, 161
- Kauffmann G. et al., 2003, *MNRAS*, 346, 1055
- Kauffman M., Grupe D., Elmegreen B. G., Elmegreen D. M., Struck C., Brinks E., 2012, *AJ*, 144, 156
- Kawabata K. S. et al., 2010, *Nature*, 465, 326
- Kelly B. C., 2007, *ApJ*, 665, 1489
- Kewley L. J., Dopita M. A., Sutherland R. S., Heisler C. A., Trevena J., 2001, *ApJ*, 556, 121
- Kewley L. J., Groves B., Kauffmann G., Heckman T., 2006, *MNRAS*, 372, 961
- Kromer M., Sim S. A., Fink M., Röpke F. K., Seitzzahl I. R., Hillebrandt W., 2010, *ApJ*, 719, 1067
- Leaman J., Li W., Chornock R., Filippenko A. V., 2011, *MNRAS*, 412, 1419
- Li W., Chornock R., Leaman J., Filippenko A. V., Poznanski D., Wang X., Ganeshalingam M., Mannucci F., 2011, *MNRAS*, 412, 1473
- Liu X., Shen Y., Strauss M. A., Hao L., 2011, *ApJ*, 737, 101
- Lu Y., Yu Q., Lin D. N. C., 2007, *ApJ*, 666, L89
- Lyman J. D., James P. A., Perets H. B., Anderson J. P., Gal-Yam A., Mazzali P., Percival S. M., 2013, *MNRAS*, 434, 527
- Lyman J. D., Levan A. J., Church R. P., Davies M. B., Tanvir N. R., 2014, *MNRAS*, 444, 2157
- Maeda K., Taubenberger S., Sollerman J., Mazzali P. A., Leloudas G., Nomoto K., Motohara K., 2010, *ApJ*, 708, 1703
- Moore B., Lake G., Katz N., 1998, *ApJ*, 495, 139
- Moore B., Lake G., Quinn T., Stadel J., 1999, *MNRAS*, 304, 465
- Nagar N. M., Falcke H., Wilson A. S., 2005, *A&A*, 435, 521
- Oke J. B. et al., 1995, *PASP*, 107, 375
- Palladino L. E., Schlesinger K. J., Holley-Bockelmann K., Allende Prieto C., Beers T. C., Lee Y. S., Schneider D. P., 2014, *ApJ*, 780, 7
- Peletier R. F., Davies R. L., Illingworth G. D., Davis L. E., Cawson M., 1990, *AJ*, 100, 1091
- Perets H. B., Gal-yam A., Crockett R. M., Anderson J. P., James P. A., Sullivan M., Neill J. D., Leonard D. C., 2011, *ApJ*, 728, L36
- Perets H. B. et al., 2010, *Nature*, 465, 322
- Quimby R. M. et al., 2011, *Nature*, 474, 487
- Sesana A., Madau P., Haardt F., 2009, *MNRAS*, 392, L31
- Shen K. J., Kasen D., Weinberg N. N., Bildsten L., Scannapieco E., 2010, *ApJ*, 715, 767
- Silverman J. M. et al., 2012, *MNRAS*, 425, 1789
- Silverman J. M., Ganeshalingam M., Filippenko A. V., 2013, *MNRAS*, 529
- Sim S. A., Fink M., Kromer M., Röpke F. K., Ruiter A. J., Hillebrandt W., 2012, *MNRAS*, 420, 3003
- Smith N., Foley R. J., Filippenko A. V., 2008, *ApJ*, 680, 568
- Smith N. et al., 2007, *ApJ*, 666, 1116
- Sullivan M. et al., 2011, *ApJ*, 732, 118
- Tanvir N. R., Levan A. J., Fruchter A. S., Hjorth J., Hounsell R. A., Wiersema K., Tunnicliffe R. L., 2013, *Nature*, 500, 547
- Tauris T. M., 2015, *MNRAS*, 448, L6
- Tremonti C. A. et al., 2004, *ApJ*, 613, 898
- Valenti S. et al., 2014, *MNRAS*, 437, 1519
- Véron-Cetty M.-P., Véron P., 2006, *A&A*, 455, 773
- Wade R. A., Horne K., 1988, *ApJ*, 324, 411
- Waldman R., Sauer D., Livne E., Perets H., Glasner A., Mazzali P., Truran J. W., Gal-Yam A., 2011, *ApJ*, 738, 21
- Yaron O., Gal-Yam A., 2012, *PASP*, 124, 668
- Yu Q., Tremaine S., 2003, *ApJ*, 599, 1129
- Yuan F., Kobayashi C., Schmidt B. P., Podsiadlowski P., Sim S. A., Scalzo R. A., 2013, *MNRAS*, 432, 1680

Table A1. Ca-rich SN Host-galaxy Demographics

SN	Host	Morphology	AGN	z	Scale (kpc/'')	Major Axis (")	Axis Ratio (b/a)	Galactic P.A. ($^{\circ}$)
2000ds	NGC 2768	E	LINER	0.0045	0.113	65.70	0.460	-87.5
2001co	NGC 5559	Sb (BGG)	BPT Comp	0.0172	0.383	18.55	0.300	60
2003H	NGC 2207	Sbc (interacting)	AGN	0.0091	0.171	36.25	0.680	70
2003dg	UGC 6934	Scd	...	0.0183	0.405	11.15	0.320	-35
2003dr	NGC 5714	Scd (BGG)	...	0.0075	0.184	28.30	0.160	80
2005E	NGC 1032	S0/a	Radio Excess	0.0090	0.173	33.80	0.400	70
2005cz	NGC 4589	E (BGG)	LINER	0.0066	0.158	34.75	0.750	92.5
2007ke	NGC 1129	E (BCG; merger)	...	0.0173	0.340	38.15	0.880	70
2010et	CGCG 170-011	E (group)	BPT AGN	0.0233	0.495	7.00	0.800	-30
2012hn	NGC 2272	S0 (BGG)	...	0.0071	0.142	25.50	0.740	-55
PTF09dav	2MASS J22465295+2138221	Disturbed Spiral	...	0.0371	0.735	4.35	0.740	-85
PTF11bij	IC 3956	S0? (BGG)	AGN	0.0347	0.720	5.45	0.900	-20
PTF11kmb	NGC 7265	S0 (BGG)	...	0.0170	0.343	26.25	0.760	-10

Table A2. Ca-rich SN Sample Demographics

SN	SN Offset (")	SN Offset (kpc)	SN Offset (Isophotal Radii)	Angle Offset ($^{\circ}$)	Velocity Shift (km s^{-1})
2000ds	33.4	3.77	1.08	76.67	-190 (30)
2001co	18.5	7.07	1.22	13.03	-470 (530)
2003H	51.0	8.73	1.52	22.47	-180 (130)
2003dg	4.1	1.66	0.39	6.05	-1120 (40)
2003dr	14.4	2.65	2.89	65.09	560 (40)
2005E	140.3	24.27	6.07	27.78	-140 (30)
2005cz	13.4	2.12	0.41	24.07	-1030 (140)
2007ke	49.2	16.71	1.31	17.31	470 (120)
2010et	76.0	37.64	10.95	9.44	-430 (70)
2012hn	47.4	6.73	2.48	75.50	-1730 (70)
PTF09dav	56.8	41.75	16.09	52.29	-110 (60)
PTF11bij	47.8	34.42	8.80	10.00	580 (100)
PTF11kmb	437.5	150.05	20.46	56.36	260 (20)